Birkeland Currents: A Force-Free Field-Aligned Model

Donald E. Scott

Department of Electrical Engineering (Retired), University of Massachusetts, Amherst, MA, USA.
e-mail: dascott3@cox.net

The fundamental vector calculus definition of a force-free, field-aligned current in space is expanded in cylindrical coordinates to directly obtain the Bessel partial differential equation that specifies the magnetic field created by such a current. This result is often called the Lundquist solution. A simple but detailed derivation is included here. The physical properties of the resulting intricate magnetic field structure are described. The cause of its characteristic counter-rotation and counter-flows are identified. The describing equations are put into state-variable form and a step-wise approximation is applied. This solution reveals the primary effect of the force-free parameter, α, as being a scale factor of radial distance. We show that: 1) both the axial and azimuthal magnetic and current density components cyclically reverse their directions with radial distance from the central axis of the current; 2) the magnetic field extends farther from the central axis within a force-free field than it would if produced by a current in a long straight conductor. The total magnetic field magnitude and current density are shown to vary inversely as the square root of r. For large r, outside the plasma, the azimuthal magnetic field is shown to vary as $1/r$. These results are shown to be consistent with laboratory and astronomical observations.

1 Introduction

After Kristian Birkeland [1] (1867-1917) suggested in 1908 that Earth's auroras were powered by corpuscular rays emanating from the Sun that become deflected into Earth's polar regions by the geomagnetic field, the existence of such magnetic field-aligned currents was strongly disputed based partially on the idea that currents could not cross the presumed "vacuum" of space [2, p. 181]. Birkeland's main problem, however, was that having made detailed measurements of Earth's geomagnetic field on the ground, he then wanted to extrapolate that knowledge into a description of the current-density distribution that caused those magnetic effects. This is not possible because a given magnetic field value can be produced by more than one distribution of current-density.

A level of interest did, however, develop regarding the Sun's photosphere and plasma properties of the solar corona. For example, a mathematical model of a force-free magnetic field was proposed as early as 1950 by Lundquist [3, 4]. He investigated whether magnetic fields could exist in an electrically conducting liquid and his results included presentation of the now well-known Bessel solution for force-free fields. Later in 1957, investigators such as Chandrasekhar and Kendall [5] applied a similar analysis to the spherical geometry of the Sun.

NASA scientists and many other investigators worked on Birkeland currents and flux rope observations since the mid-to-late 1960's [6–18], with substantial activity on this topic after the late 1980's [19–24]. A few researchers have sought cylindrical coordinate solutions [25] but almost always in reference to intricate quasi-cylindrical solar surface or coronal applications. Potemra [24] concluded that Birkeland currents and Alfvén waves are fundamental to an understanding of the Earth's plasma environment. It is now generally assumed that magnetic fields inside interplanetary magnetic clouds and flux ropes in the solar photosphere are force-free [26]. In 2009, space probe Themis discovered a flux rope pumping a 650,000 A current down into the arctic auroral region [27]. This strong observational evidence supports the existence of Birkeland Currents.

Consistent with this, the major goals of this paper are:

1. To present a simple, but complete derivation of Lundquist's equations that describe the magnetic field structure of a field-aligned current.
2. To fully describe the physical (not only magnetic, but also both the electrical and structural) consequences of those equations; to develop a model.
3. To demonstrate the correspondence between the properties of that model and observational evidence gathered from both plasma laboratories and astronomical images.

First we show that the basis of any model of a Birkeland current is what is called a force-free, field-aligned current.

2 Definition of a force-free field-aligned current

Consider a stream of moving charged particles (an electrical current) in a plasma that is not subject to any external forces. A useful mathematical idealization of such a physical cosmic current is a vector field of current density, $\boldsymbol{j}$, that, when viewed in a cylindrical coordinate system, creates an overall average current vector, $\boldsymbol{I}$, which, by definition determines the direction of the z-axis. The magnitude of $\boldsymbol{I}$ is assumed to be everywhere independent of the z coordinate. The coordinate system defines a point, p, represented by (r, θ, z), as illustrated in Figure 1.

The basic structure of such a cosmic magnetic field is controlled by the momentum equation of ideal magneto-hydrodynamics [25, 28–30],

$$(\nabla \times \boldsymbol{B}) \times \boldsymbol{B} = \mu_0 \nabla p \tag{1}$$

where μ_0 is the permeability of free-space.

The left hand side of this expression represents the compressive magnetic (Lorentz) force and the right side is the expansive force (pressure gradient multiplied by the permeability of the plasma). We distinguish between force-free fields with $\nabla p = 0$ and pressure balanced fields with $\nabla p \neq 0$. On the photosphere and within the lower chromosphere of the Sun the energy of the plasma motion dominates the magnetic energy and therefore the field is swept passively along with the plasma. This condition is characterized as a high-β plasma [31], where the parameter β is defined as the ratio between the plasma pressure p and the magnetic pressure,

$$\beta = 2\mu_0 \frac{p}{\boldsymbol{B}^2}. \tag{2}$$

Higher up in the corona, in interplanetary and in cosmic space, a lower pressure (lower ion and electron densities), low-β plasma often exists depending on local field pressure. Here the plasma can take on a force-free character [6,32,33]. However, care must be exercised in assuming low-β properties. For example, "*the extensive magnetosheath flow downstream of Earth's bow shock is a high-beta plasma. Along a radial cut of the plasma coming inward from the Sun near the dayside sub-solar point, the solar wind and magnetosheath flow is high-beta, the magnetopause and immediate (thin) plasma boundary provides a high to low beta transition, and immediately within the low-latitude boundary layer (within the outer magnetosphere) plasma is low-beta. Then with lower radial distance the plasma again becomes high-beta.*" [34]. We now present here a model that requires a low-β plasma environment.

The electromagnetic force experienced by each charge within such a plasma is given by,

$$\boldsymbol{F} = q(\boldsymbol{E} + \boldsymbol{v} \times \boldsymbol{B}). \tag{3}$$

The first term, $q\boldsymbol{E}$, is the *electric force* and the second term, $q(\boldsymbol{v} \times \boldsymbol{B})$, is called the *magnetic force*. The name *Lorentz force* is used to describe expression (3). The plasma region contains the cylindrical current stream. No initial assumptions are made about the distribution of the current density across the cross-section.

A flow of charge creates its own magnetic field through which the charge flows. The site at which each charged particle, q, in the stream is located is the point of origin of two local vectors: $\boldsymbol{j} = q\boldsymbol{v}$ (current density) and $\boldsymbol{B}$ (magnetic field). The current density vector $\boldsymbol{j}$ at each point inherently creates a *curl*($\boldsymbol{B}$) vector given by Maxwell [35]:

$$\nabla \times \boldsymbol{B} = \mu \left(\boldsymbol{j} + \epsilon \frac{\partial \boldsymbol{E}}{\partial t} \right). \tag{4}$$

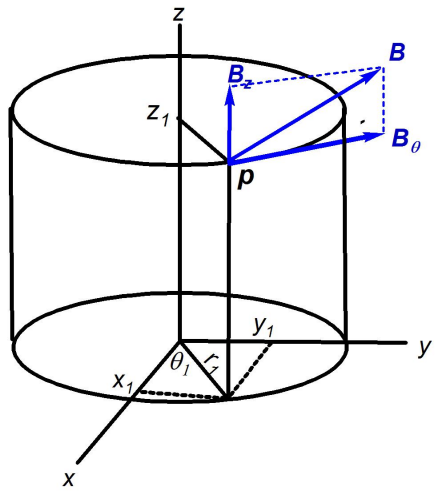

Fig. 1: Total magnetic field vector $\boldsymbol{B} = \boldsymbol{B}(r, \theta, z)$, and its two components B_z and B_θ at a particular location; $B_r = 0$. Note that at any point r, the pitch angle of the vector $\boldsymbol{B}$ measured upward from the horizontal plane is defined as the arctan $[B_z(r)/B_\theta(r)]$.

The derivative term in (4) which was added by Maxwell is called the displacement current. It is often considered to be zero valued, as we do here, when it can be assumed there are no time-varying electric fields in the region. Integrating the *curl*($\boldsymbol{B}$) vectors over a cross-section of the cylindrical stream (Stoke's theorem) yields,

$$\int_S \nabla \times \boldsymbol{B} \cdot d\boldsymbol{S} = \int_S \mu \boldsymbol{j} \cdot d\boldsymbol{S} = \oint_C \boldsymbol{B} \cdot d\boldsymbol{l} \tag{5}$$

where S is any cross-section of the plasma, and μ and ϵ are the permeability and permittivity respectively of the plasma medium. The second term in (5) is equivalently $\mu\boldsymbol{I}$ where $\boldsymbol{I}$ is the total current carried by the plasma. If the cross-section is circular with radius r, then the last term in (5) is $2\pi r\boldsymbol{B}$ where $\boldsymbol{B}$ is in the azimuthal, θ, direction, not aligned with $\boldsymbol{I}$ and the z-axis. Thus the $\boldsymbol{B}$ field produced by a cylindrical plasma at its outer boundary, $r = R$, is

$$\boldsymbol{B}_\theta = \frac{\mu \boldsymbol{I}}{2\pi R}. \tag{6}$$

Expression (4) is the *point form* and (5) is the *integral (macroscopic) form* of that Maxwell equation. Expression (4) is valid at any point. The integral forms given in (5) and (6) imply that $\boldsymbol{B}$ is a vector sum of the effects of all the $\boldsymbol{j}$ vectors on the surface $\boldsymbol{S}$ that is enclosed by C. $\boldsymbol{B}$ is not directly produced by any single $\boldsymbol{j}$. In (4) it is clear that $\boldsymbol{j}$, the current density at a point, creates only a single *curl*($\boldsymbol{B}$) vector, not a $\boldsymbol{B}$ vector. In general, there can be (and often is) a non-zero valued $\boldsymbol{B}$ vector at points at which $\boldsymbol{j} = \boldsymbol{0}$.

Prior to the time a cosmic current system, free of externally applied forces or fields, reaches a steady-state config-

uration, the $\boldsymbol{j}$ and $\boldsymbol{B}$ vectors are interacting – all the $\boldsymbol{j}$'s are creating *curl*($\boldsymbol{B}$) vectors that sum to form the local $\boldsymbol{B}$ vectors. At any point in the plasma where $\boldsymbol{j} \neq \boldsymbol{0}$ a force can exist between that current density vector and its local magnetic $\boldsymbol{B}$-field vector. This force is a magnetic *Lorentz force* given by the second term in (3). This vector cross product of a moving charge's velocity vector $\boldsymbol{v}$ and the local vector $\boldsymbol{B}$ implies that the scalar value (magnitude) of the resulting Lorentz force on each q is given by,

$$F_L = qvB\sin\varphi \tag{7}$$

where φ is the smallest angle between the vectors $\boldsymbol{v}$ and $\boldsymbol{B}$, with scalar values v and B. We call φ the Lorentz angle. If this angle is zero or 180 degrees, the magnetic Lorentz $\boldsymbol{v}\times\boldsymbol{B}$ force at that point is zero-valued.

The *magnetic intensity* (symbol $\boldsymbol{H}$) is often used to describe the macroscopic forcing function that creates a magnetic field,

$$H = \frac{B}{\mu} = \frac{NI}{l}. \tag{8}$$

The dimensions of $\boldsymbol{H}$ are A/m. (The number of turns, N, is dimensionless). $\boldsymbol{H}$ has also been called the *magnetic field strength*, and the *magnetizing force*.

The scalar magnitude, B, in (8) arises from the integral form (5). In that expression, B is shown to be the result of the total current, I. It follows that H is not a point form variable.

It may be shown that the energy density, W_B (Joules/m^3), stored in the magnetic field of such a current stream is given by,

$$W_B = \frac{\mu}{2}H^2. \tag{9}$$

Using (8) in (9), the total energy stored, ψ (Joules), in the magnetic field of a cosmic current is given by,

$$\psi = \frac{1}{2}\left(\frac{\mu N^2 A_c}{l}\right)I^2 \tag{10}$$

where A_c is the cross-sectional area and the *inductance* of the current stream is defined by the factor in parentheses. This shows that the only way to reduce the entire stored energy to zero is to completely cut off the current (set $I = 0$); in which case the entire cosmic current structure would cease to exist.

However, we assume that in unconstrained plasma in cosmic space, the current stream is free to move and distribute itself so as to minimize the internally stored potential energy due to the stresses resulting from magnetic Lorentz forces everywhere throughout the plasma. In fact space plasmas are uniquely situated to obey the *minimum total potential energy principle* [36], which asserts that a system or body shall deform or displace to a position and/or morphology that minimizes its total potential (stored) energy (a formalization of the idea that "water always flows downhill.").

The energy described in (10) is irreducible because it is caused by the fixed quantity, I. But the Lorentz energies can be eliminated because they do not depend on the value of I, only on the cross-products between local $\boldsymbol{B}$ and $\boldsymbol{j}$ vectors.

If and when the process of shedding the internal magnetic-force energy reaches a steady-state equilibrium, this structure is called a *force-free current* and is defined by the relation between the magnetic field vector, $\boldsymbol{B}$, and the current density vector, $\boldsymbol{j}$, at every location at which a charge, q, exists in the current stream:

$$q(\boldsymbol{v}\times\boldsymbol{B}) = \boldsymbol{j}\times\boldsymbol{B} = 0. \tag{11}$$

It follows from (11) that the Lorentz forces are everywhere equal to zero in a force-free current because every $\boldsymbol{j}$ is collinear with its corresponding $\boldsymbol{B}$. This arrangement is therefore also called a *field-aligned current* (FAC).

It follows directly from (4) and (11) that, if there is no time-varying electric field present, then (11) is equivalent to

$$(\nabla\times\boldsymbol{B})\times\boldsymbol{B} = 0 \tag{12}$$

which is identical to (1) with $\nabla p = 0$. This is the basic defining property of a force-free, field-aligned current.

Expression (4) implies that, if at any point in an otherwise field-aligned current, $\boldsymbol{j} = \boldsymbol{0}$, (12) is automatically fulfilled even if $\boldsymbol{B}$ is non-zero. The value of the magnitude and direction of $\boldsymbol{B}$ at any given point is generally not sufficient information to determine the magnitude, direction, or even the existence of $\boldsymbol{j}$ at that point. This is the problem that confronted Birkeland in his attempts to identify the currents responsible for the magnetic field variations he measured. However, from (4), knowledge of the direction and magnitude of the $\nabla\times\boldsymbol{B}$ vector at any given point does identically determine the value of $\mu\boldsymbol{j}$ there.

Field-aligned, force-free currents represent the lowest state of stored magnetic energy attainable in a cosmic current [31]. We seek an expression for the magnetic field, $\boldsymbol{B}(r,\theta,z)$, in such a current/field structure.

3 Quantitative model of a force-free field-aligned current

Equation (12) can be expanded into differential equation form using the cylindrical coordinate definition of curl and the 3-dimensional vector product determinant. However, this leads to an expression of little utility. Because (12) is satisfied if the current density, $\boldsymbol{j}$, has the same direction (except for sign) as $\boldsymbol{B}$ (and with no requirements on its magnitude), it was suggested (Lundquist [3, 4] and many others) that,

$$\nabla\times\boldsymbol{B} = \alpha\boldsymbol{B} \tag{13}$$

which from (4) is equivalently,

$$\mu\boldsymbol{j} = \alpha\boldsymbol{B} \tag{14}$$

where α is any non-zero valued scalar, which is equivalent to (12). This leads to a simple solution, but it is important

to note that accepting (14) as a substitute for (12) assumes *a priori* that, for any non-zero α, a non-zero valued $\boldsymbol{B}$ at any point requires the existence of a current density $\boldsymbol{j} \neq \boldsymbol{0}$ at that same point. This is in general, an unwarranted presumption. This is especially so in light of the well-known tendency of plasmas to form filaments (creating regions where $\boldsymbol{j} = \boldsymbol{0}$ but $\boldsymbol{B}$ is not). There are many examples in the study of electromagnetism, such as: Given that, in otherwise empty space, a current, $I_x = +1$ A exists in a straight, infinitely long conductor lying along the x-axis, find the value of the resulting magnetic field vector, $\boldsymbol{B}$, at the point $(x = y = 0, z = 1)$. The goal of this exercise is to find a value of $\boldsymbol{B}$ at a point where $\boldsymbol{j}$ is explicitly zero-valued. The answer is not zero.

However, most investigators start unhesitatingly with (13) and therefore (14) as givens. (This rules out applying the solution to a filamented plasma.) For example, Wiegelmann [37] does this and derives a vector Helmholtz equation which he states, can be solved by a separation *ansatz*, a Green's function method [8] or a Fourier method [18].

An *ansatz* is the establishment of the starting equation(s), the theorem(s), or the value(s) describing a mathematical or physical problem or solution. After an *ansatz* has been established (constituting nothing more than an assumption), the equations are solved for the general function of interest (constituting a confirmation of the assumption). That the mathematical solution accurately describes the physics is assumed.

In his 1950 paper Lundquist (after accepting the validity of (13)), without further explanation or derivation states that the solution of (14) with constant α is,

$$\begin{aligned} H_z &= A\, J_0(\alpha r) \\ H_\theta &= A\, J_1(\alpha r). \end{aligned} \tag{15}$$

Lundquist thus presents α as being a radial distance scale factor in the argument of his Bessel function solution. No evaluation of the coefficient A is offered. He also presents an image similar to Figure 6 below, but does not derive the current density or the physical consequences of these functions such as periodic reversals with increasing radius or counter-rotation and counter-flows of the plasma within the current structure.

Other investigators [45] start with (13) and then take its curl to obtain,

$$\begin{aligned} \nabla(\nabla\cdot\boldsymbol{B}) - \nabla^2\boldsymbol{B} &= \alpha(\nabla\times\boldsymbol{B}) \\ \nabla^2\boldsymbol{B} &= -\alpha(\nabla\times\boldsymbol{B}). \end{aligned} \tag{16}$$

They then also present the solution of (16) as being that given in (15). This agrees with Lundquist.

One of the most extensive reviews of force-free currents in a cylindrical geometry by Botha & Evangelidis [25] contains several references to similar studies. However, none of these investigators make the simplest assumptions: adopt a piece-wise linear approach, assume α to be any scalar value, and assume no variation of $\boldsymbol{j}$ or $\boldsymbol{B}$ in either the azimuthal or axial directions. Such simplifications may not be justified on the solar surface, but are in deep space. Therefore, we derive here a simple solution that follows from this and carefully note the effect of the parameter α on the resulting model.

Before beginning this derivation, we specify the dimensions of several involved quantities. Using (8),

$$[\mu] = \left[\frac{B}{H}\right] = \frac{\mathrm{Wb}}{\mathrm{m}^2}\frac{\mathrm{m}}{\mathrm{A}} = \frac{\mathrm{Wb}}{\mathrm{mA}}. \tag{17}$$

Using (4) the following units obtain,

$$[\nabla\times\boldsymbol{B}] = [\mu j] = \frac{\mathrm{Wb}}{\mathrm{mA}}\frac{\mathrm{A}}{\mathrm{m}^2} = \frac{\mathrm{Wb}}{\mathrm{m}^3}. \tag{18}$$

Using (13),

$$\frac{\mathrm{Wb}}{\mathrm{m}^3} = [\alpha]\frac{\mathrm{Wb}}{\mathrm{m}^2} \tag{19}$$

or

$$[\alpha] = 1/\mathrm{meter}. \tag{20}$$

Our derivation is as follows: The left side of (13) is expanded in cylindrical coordinates:

$$\begin{aligned} \nabla\times\boldsymbol{B} = \Bigg(&\frac{1}{r}\frac{\partial B_z}{\partial\theta} - \frac{\partial B_\theta}{\partial z}, \frac{\partial B_r}{\partial z} - \frac{\partial B_z}{\partial r}, \\ &\frac{1}{r}\frac{\partial}{\partial r}(rB_\theta) - \frac{1}{r}\frac{\partial B_r}{\partial\theta}\Bigg) \end{aligned} \tag{21}$$

and the right side of (13) is expressed as,

$$\alpha\boldsymbol{B} = (\alpha B_r, \alpha B_\theta, \alpha B_z). \tag{22}$$

In (21) and (22), all field components are functions of the position vector, $\boldsymbol{p}$. Given that there is no reason to assume any variation of current density $\boldsymbol{j}$ in the θ or z directions in cosmic space, (14) implies the same is true for $\boldsymbol{B}$.

It follows from the absence of any externally applied forces other than possibly a static axial electric field to maintain $\boldsymbol{I}$ (first term in (3)) and any time-varying electric fields, that all partial derivatives of $\boldsymbol{B}$ with respect to θ and z are zero and, therefore, what remains of (13) after these simplifications in (21) are the following three expressions: In the radial direction,

$$\alpha\boldsymbol{B}_r = 0. \tag{23}$$

There is no radial component of the $\boldsymbol{B}$ vector. This is consistent with Maxwell's $\nabla\cdot\boldsymbol{B} = 0$. In the azimuthal direction,

$$\frac{\partial B_z}{\partial r} = -\alpha B_\theta \tag{24}$$

and in the axial direction,

$$\frac{1}{r}\frac{\partial}{\partial r}(rB_\theta) = \alpha B_z. \tag{25}$$

This results in two non-trivial coupled differential equations in the two dependent variables B_z and B_θ as shown in (24) and (25). The independent variable in both is radial distance, r.

4 Solution in closed form

Combining (24) and (25) yields a single second-order differential equation in a single dependent variable,

$$r^2 \frac{\partial^2 B_z(r)}{\partial r^2} + r \frac{\partial B_z(r)}{\partial r} + \alpha^2 r^2 B_z(r) = 0. \tag{26}$$

The dependent variable $B_z(r)$ is the axial component of the force-free steady-state magnetic field. The component field $B_z(r)$ is allowed to extend as far as the differential equation (26) provides for. No boundary condition at any non-zero value of r is introduced. There will be, in all real currents in space, a natural limit, $r = R$, to the extent of the current density $\boldsymbol{j}(r)$.

Having now fully specified the differential equation (26), it is recognized as being identical to Bessel's equation of order zero, with scalar parameter α (the units of which are (see (20)) the reciprocal of the units of r). We thus have a closed-form solution for the dependent variable in that differential equation that results from expanding equation (13). Its solution is,

$$y = AJ_0(\alpha x) + CY_0(\alpha x). \tag{27}$$

$J_0(x)$ is the Bessel function of the first kind and zero$^{\text{th}}$ order, and $Y_0(x)$ is the Bessel function of the second kind (or sometimes called the Weber or Neumann function) of zero$^{\text{th}}$ order.

The function $J_0(\alpha x)$ has the value unity at the boundary $x = 0$, and the function $Y_0(\alpha x)$ has a singularity at this same boundary. Because reality dictates that the magnetic field remain finite-valued, the value of arbitrary coefficient C must be set equal to zero. Thus, the solution to (26) is given by,

$$B_z(r) = B_z(0) J_0(\alpha r). \tag{28}$$

This Bessel function of the first kind and of order zero is used to produce Bessel functions of the first kind and orders 1, 2, 3, ... by simple differentiation. The recursion relation for the first-order Bessel function is,

$$J_1(x) = -\frac{dJ_0(x)}{dx}. \tag{29}$$

Thus, from (24) and (29), we obtain,

$$B_\theta(r) = B_z(0) J_1(\alpha r). \tag{30}$$

Consequently, from (28) and (30), the scale of the size, r, of the magnetic field in the radial direction is determined by the parameter α. Allowing $\alpha = \alpha(r)$ would distort the radial axis used to plot $B_z(r)$ and $B_\theta(r)$.

These Bessel functions approach damped trigonometric functions for large r, but the amplitude decrease is unusually gradual – varying inversely as the *square root* of αr, which is a more gradual decay than the typical exponential, or $1/\alpha r$, or $1/(\alpha r)^2$ damping.

This decay behavior is seen from the asymptotic forms shown here in (31) below,

$$\begin{aligned} J_0(x) &= \sqrt{\frac{2}{\pi x}}\left[\cos\left(x - \frac{\pi}{4}\right) + O\left(\frac{1}{x}\right)\right] \\ J_1(x) &= \sqrt{\frac{2}{\pi x}}\left[\cos\left(x - \frac{3\pi}{4}\right) + O\left(\frac{1}{x}\right)\right]. \end{aligned} \tag{31}$$

Therefore, $B_r(r)$, $B_z(r)$ and $B_\theta(r)$ shown in (23), (28), and (30) together provide a complete description of the magnetic field that surrounds and pervades the final force-free, minimum-energy, steady-state, cylindrical current. In this state, all Lorentz forces have been reduced to zero. The physical implications of these expressions are fully described in Section 8, below.

5 Euler method of solution

Another approach to solving (26), one that does not require that it be recognized as a Bessel equation, is to use an iterative numerical method. One such method is based on a *state-variable representation* of the differential equation – in this case the pair (24) and (25). In order to describe those differential equations in state-variable form, the product rule for derivatives is first applied to (25) as follows:

$$\frac{\partial(rB_\theta)}{\partial r} = r\alpha B_z \tag{32}$$

$$r\frac{\partial B_\theta}{\partial r} + B_\theta = r\alpha B_z. \tag{33}$$

Two state-variables may be defined as follows:

$$x_1 = B_z \tag{34}$$

$$x_2 = B_\theta \tag{35}$$

so that rewriting (24) and (25) in state-variable form yields,

$$\frac{dx_1}{dr} = -\alpha x_2 \tag{36}$$

$$\frac{dx_2}{dr} = \alpha x_1 - \left(\frac{1}{r}\right) x_2. \tag{37}$$

An Euler/Runge-Kutta algorithm for obtaining an approximate step-wise solution to (36) and (37) was implemented. The results, presented in Figure 2, show, as expected, the familiar shapes of Bessel functions J_0 and J_1 as $B_z(r)$ the axial component, and $B_\theta(r)$ the azimuthal component. Also shown is the total magnetic field strength $|\boldsymbol{B}|$ (the square root of the sum of the squares of the two component scalar fields, B_z and B_θ). This total field strength magnitude is strongest at a minimum radial value r and decreases monotonically with increasing r.

Specifically, in Figure 2, *total magnetic field magnitude* is shown to decrease with increasing radial distance from the

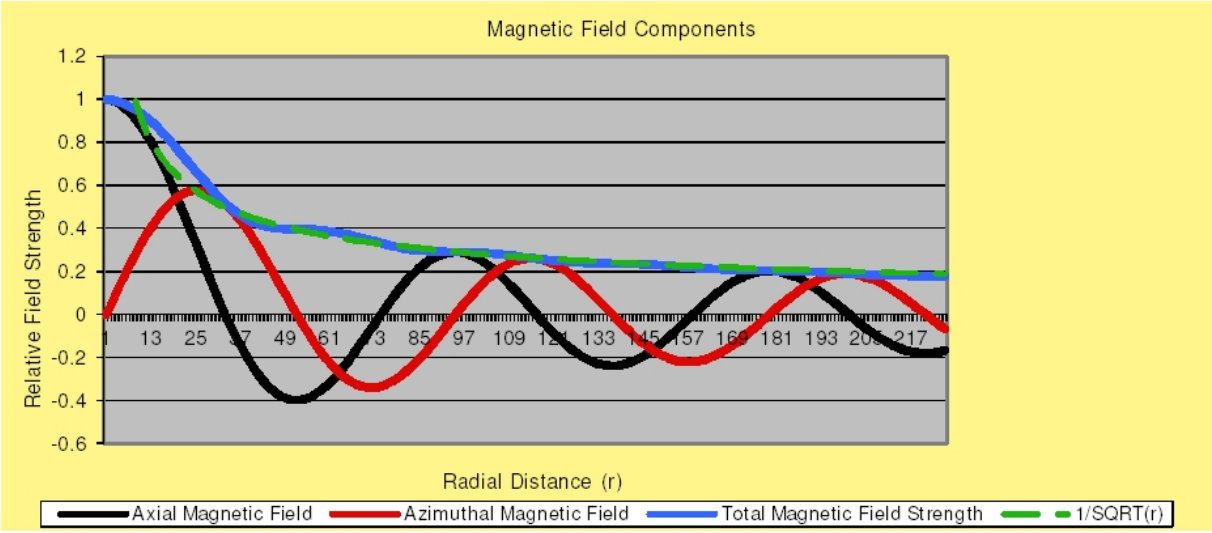

Fig. 2: Axial Magnetic Field component B_z, the Azimuthal Magnetic Field component B_θ, the magnitude of the Total Magnetic Field; and, for reference, a plot of $1/\sqrt{r}$ – all vs. radial distance quantized to integer multiples of the step-size h = 0.1. The value of α arbitrarily selected in (36) and (37) to achieve adequate resolution of the Bessel functions with this step-size is 0.075. The horizontal axis in this plot is the radius r-axis. Note in Table I that in every case (row) the inherently dimensionless Bessel function argument, $x = \alpha r$, thus demonstrating the scale factor utility of α. (e.g., $2.4048 = 0.075 \times 32$.)

central axis of the current as $(\alpha r)^{-1/2}$. This function is shown, for reference, as the fourth series plotted in Figure 2. This behavior was fully described in Section 4 (see (31)). Therefore, the magnetic fields within field-aligned cosmic currents clearly extend outward in space much farther and less diminished in strength than the magnetic field that would be generated by a simple straight-wire electric current (see (6)).

The parameter α appears as a scale factor operating on the radius variable, r. In the result shown in Figure 2, the value for that distance-scaling parameter was arbitrarily chosen to be $\alpha = 0.075$. The horizontal axis of Figure 2 is in units of actual radial distance, r. For example, the first zero of $J_0(x)$ is located at $x = 2.4048$. In Figure 2 it is shown to occur at $r = x/0.075 = 32$. This demonstrates the relationship between the non-dimensional argument of the Bessel functions, x, and the scaled variable, r: $x = \alpha r$. Nothing is inferred or implied about the current density vector field $\boldsymbol{j}$ at this stage.

The step-wise Euler method described here can also be used in the event the state-equations are nonlinear due to choosing an arbitrary $\alpha = \alpha(r)$.

6 General validity of solution

A question remains regarding the generality of the solutions (23), (28), and (30), for $B_r(r)$, $B_\theta(r)$, and $B_z(r)$ respectively. Directly or indirectly all three of these quantities result from solving the Bessel equation (26), which, itself, is derived from the substitute equation (13), not from the fundamental, definition of a *force-free current* (12). This substitute, (13), was posited as being a valid alternative to (12), the defining property. Expressions (12) and (13) impose similar but not identical requirements on the magnetic field $\boldsymbol{B}(r, \theta, z)$ and the current density field $\boldsymbol{j}(r, \theta, z)$. Therefore, it has not yet been demonstrated that the vector field solutions of (13) listed in (23), (28) and (30) are also valid solutions of the fundamental definition, (12).

Table 1: IMPORTANT VALUES FOR RADIAL MAGNETIC COMPONENTS

Radius Values $r = x/\alpha$	Zeros of $J_0(x)$ X	Zeros of $J_1(x)$ x	Description
0		0	B_z pos max, B_θ zero
32	2.4048		B_z zero, B_θ pos max
51		3.8317	B_z neg max, B_θ zero
74	5.5201		B_z zero, B_θ neg max
94		7.0156	B_z pos max, B_θ zero
116	8.6537		B_z zero, B_θ pos max
136		10.1735	B_z neg max, B_θ zero
158	11.7915		B_z zero, B_θ neg max
178		13.3237	B_z pos max, B_θ zero
199	14.9309		B_z zero, B_θ pos max

In order to demonstrate this, we insert those solutions back into (12) by writing the central three-dimensional cross product contained in that expression in determinant form:

$$(\nabla \times \boldsymbol{B}) \times \boldsymbol{B} = \begin{vmatrix} \hat{r} & \hat{\theta} & \hat{z} \\ (\nabla \times \boldsymbol{B}_r) & (\nabla \times \boldsymbol{B}_\theta) & (\nabla \times \boldsymbol{B}_z) \\ \boldsymbol{B}_r & \boldsymbol{B}_\theta & \boldsymbol{B}_z \end{vmatrix}. \quad (38)$$

Using the cylindrical curl expansion of (21),

$$\left|\mathrm{b}_{ij}\right| = (\nabla \times \boldsymbol{B}) \times \boldsymbol{B} = \begin{vmatrix} \hat{r} & \hat{\theta} & \hat{z} \\ 0 & -\frac{\partial B_z}{\partial r} & \frac{1}{r}\frac{\partial}{\partial r}(rB_\theta) \\ B_r & B_\theta & B_z \end{vmatrix}. \quad (39)$$

We use (23), (28) and (30). Then in (39) the element b_{22} becomes,

$$\begin{aligned} b_{22} &= -\frac{\partial}{\partial r}\left[B_z(0)\,J_0(\alpha r)\right] \\ &= \alpha B_z(0)\,J_1(\alpha r)\,. \end{aligned} \tag{40}$$

The element b_{23} becomes,

$$\begin{aligned} b_{23} &= \frac{1}{r}\left(r\frac{\partial B_\theta}{\partial r}+B_\theta\right) = \frac{\partial B_\theta}{\partial r}+\frac{1}{r}B_\theta \\ &= \alpha B_z(0)\left[\frac{\partial J_1(\alpha r)}{\partial r}+\frac{1}{\alpha r}J_1(\alpha r)\right]. \end{aligned} \tag{41}$$

Since

$$\frac{\partial J_1}{\partial x} = J_0 - \frac{1}{x}J_1, \tag{42}$$

(41) becomes,

$$\begin{aligned} b_{23} &= \alpha B_z(0)\left[J_0(\alpha r)-\frac{1}{\alpha r}J_1(\alpha r)+\frac{1}{\alpha r}J_1(\alpha r)\right] \\ &= \alpha B_z(0)\,J_0(\alpha r)\,. \end{aligned} \tag{43}$$

Using the above expressions together with (23), (28), and (30), in (39) and omitting functions' arguments for clarity,

$$(\nabla\times\boldsymbol{B})\times\boldsymbol{B} = \begin{vmatrix} \hat{r} & \hat{\theta} & \hat{z} \\ 0 & \alpha B_0 J_1 & \alpha B_0 J_0 \\ 0 & B_0 J_1 & B_0 J_0 \end{vmatrix} = \mathbf{0}. \tag{44}$$

(QED)

Thus, the components of $\boldsymbol{B}(r,\theta,z)$ given in (23), (28), and (30) are shown to be valid solutions of the original defining equation (12). That fact remains valid whether or not the alternative (13) had ever been suggested.

Regarding the practical evaluation of α when approximate observations of both $\boldsymbol{B}$ and $\nabla\times\boldsymbol{B}$ are available, we have [31, p.107],

$$\alpha = \frac{(\nabla\times\boldsymbol{B})\cdot\boldsymbol{B}}{B^2}. \tag{45}$$

Inserting the appropriate components from (23), (28), and (30) into (45) yields the identity,

$$\alpha = \alpha. \tag{46}$$

This indicates that the results presented here as (23), (28) and (30) are consistent with the formulation for α given in (45).

7 Current density of a field aligned current

Having accepted the postulated alternative definition (13) and (14) to determine the force-free magnetic-field solutions (28) and (30) (repeated below as (47) and (48)), it is then logically consistent to simply insert these into (14) to obtain the companion current-density relations (49) and (50):

$$B_z(r) = B_z(0)\,J_0(\alpha r) \tag{47}$$

$$B_\theta(r) = B_z(0)\,J_1(\alpha r) \tag{48}$$

$$j_z(r) = \frac{\alpha B_z(0)}{\mu}\,J_0(\alpha r) \tag{49}$$

$$j_\theta(r) = \frac{\alpha B_z(0)}{\mu}\,J_1(\alpha r)\,. \tag{50}$$

A dimensional analysis of (49) and/or (50) using (18) and (20) shows the units of the constant term $\alpha B_z(0)/\mu$ to be $\mathrm{A/m^2}$ as they must be.

In (49) and (50), it is clear that as the radial size of the model is increased (by decreasing the value of α), the magnitude of both current density components decrease proportionally.

Wiegelmann [37] ***defines*** α as being $\alpha(x,y) = \mu_0 j_0/B_0$ (see (49) and (50)). This definition also has units of 1/m (reciprocal of distance) (see (17)-(20)). Peratt [31, p.107] states that α is adjusted until reasonable agreement is obtained with observations (see (45) and (46)).

8 Consequences of the oscillatory nature of the Bessel (Lundquist) solution

Expressions (47)–(50) fully describe the structure of the model of a minimum (Lorentz force) energy, cylindrical, force-free, field-aligned current (FAC) under the assumption of equation (14). Thus:

1. There are no points within the plasma where $\boldsymbol{B}=\mathbf{0}$. A non-zero valued magnetic field exists at every point. In the first paragraph after (3) it was stated, nor are any assumptions made about the distribution of the current density across the cross-section. (49) and (50) now express that spatial distribution of $\boldsymbol{j}(\boldsymbol{p})$.
2. At every point in the plasma, $\boldsymbol{j}$ and $\boldsymbol{B}$ are collinear.
3. At every point in the plasma $\mu\boldsymbol{j} = \alpha\boldsymbol{B}$ (assumption, as discussed in Section 3).
4. The model expressions (47)–(50) remain valid only over the range $0 < r < R$. Farther out from the z-axis than $r = R$, $\boldsymbol{j}=\mathbf{0}$. From that point outward, the cylindrical plasma appears more and more like a single straight, isolated current-carrying wire. So beyond radius R, the magnetic field strength will decay approaching $1/r$. This is shown directly using (14): for $r > R$, $\boldsymbol{j}=\mathbf{0}$, $\alpha = 0$. Then using (32) and (33) yields:

$$B_\theta(r) = \frac{k_z}{r}. \tag{51}$$

This is consistent with (6).

Visualizing this field configuration with the aid of Figures 2, 3, and 5, reveals that, within the plasma, at increasing radial values, the magnetic field, together with its collinear current density, wrap the axis of the current stream with a continuously increasing helical pitch angle.

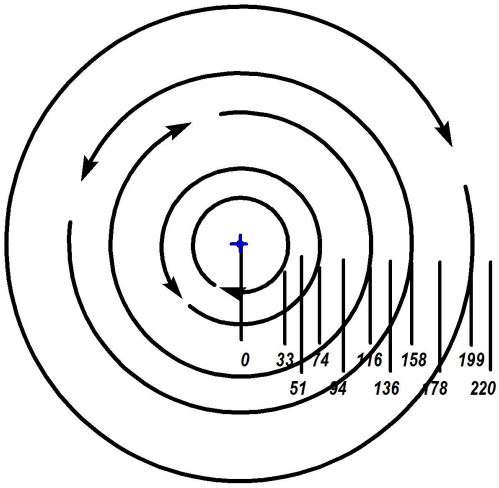

Fig. 3: Cross-section of a force-free current. In this view the reader is looking in the $+z$-direction, in the direction of main current flow. The radius values shown are plotted as values of $r = x/\alpha$ ($\alpha = 0.075$), which were used in the Euler iterative solution of (36) and (37). At the radius values shown, the axial $\boldsymbol{B}$-field is zero-valued so the total field is only azimuthal (either clockwise or counter-clockwise circles).

From (23), there is no outward radiation of the magnetic field (nor its collinear $\boldsymbol{j}$) from inside the plasma where $\alpha \neq 0$. There is no non-zero B_r or j_r component anywhere. Thus no matter escapes from the plasma. This preserves the structural integrity of the FAC over large axial distances.

Both solutions (closed-form and Euler) demonstrate repeated reversals in the directions of both the axial and the azimuthal magnetic field components with increasing radial distance. This implies the existence of a discrete set of virtual concentric cylindrical surfaces (see Figure 3). These surfaces are centered on the z-axis of the field-aligned current. At these discrete radial values, the axial field component, B_z is zero-valued and the azimuthal magnetic component, B_θ, is at alternatingly clockwise and counter-clockwise maxima. As a function of r the axial and azimuthal field strengths are observed to be in quadrature. For example in Figure 2, in a region such as that between radial distances 74 and 116, the axial field, B_z, is unidirectional (in the positive z-direction, attaining maximum strength at $r = 94$); whereas the azimuthal field reverses direction at $r = 94$, changing from the negative direction of θ to the positive direction. This results in a total magnetic field vector that wraps the current stream, its pitch angle rotating (with increasing r) in a clockwise direction when viewed looking inward in a radial direction, toward the central axis of the current (see Figure 5).

Thus, the axis of a cosmic, field-aligned current is wrapped with a compound helical magnetic field whose angle with respect to the $+z$-axis increases continuously with increasing radial distance, r. This gives rise to a structure suggestive of some ancient Roman fasces.

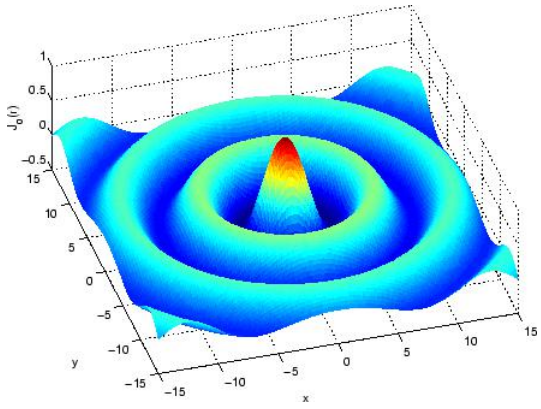

Fig. 4: Three-dimensional plot of the magnitude of the axial magnetic field component $B_z(r)$ and the current density $j_z(r)$. This demonstrates the relative strength of both those central (on-axis) fields. The magnitude scale of the horizontal axes used in this Figure are both x, the dimensionless arguments of the Bessel $J_0(x)$ and $J_1(x)$ functions.

In Figure 5, one cycle (0°–360°) of the pitch angle is shown. The cycle is sketched at eleven incrementally increasing sample values of radius. The shaded arrows show the total magnetic field direction at each value of radius, r, and the white arrows show the field direction at an increment just below each of those values of radius. At every point in a stable force-free, field-aligned current, the current density $\boldsymbol{j}$ is collinear with $\boldsymbol{B}$.

The Lundquist-Alfvén image shown in Figure 6, which is often used to describe the Birkeland current steady-state minimum-energy magnetic field, is in agreement with these results (47–50), but it only describes the morphology for small values of r. As r increases beyond what is shown in Figure 6, an uninterrupted rotation of the pitch angle of the magnetic/current helices continues (see Figure 5). The field rotation does not abruptly stop at 90° (where the total magnetic field is orthogonal to the direction of z) as might be inferred from Figure 6. The helical wrapping of the $\boldsymbol{j}$ and $\boldsymbol{B}$ fields continues with increasing radius values. This adds strength to the overall FAC structure. The tangent of the helical angle at any point, r, is the ratio (see Figure 1),

$$\frac{B_z(r)}{B_\theta(r)} = \frac{J_0(\alpha r)}{J_1(\alpha r)} = \frac{J_0(x)}{J_1(x)}. \tag{52}$$

Therefore if the value of the scale factor, $\alpha = x/r$ is, say, doubled, then that same pitch angle will occur at a value of r at half the original radius (x value unchanged). Thus the scale of the entire model will be halved (see Figure 6).

9 Effects of increased axial current

In a geomagnetic storm, a surge in the flux of charged particles (current increase) often temporarily alters Earth's magnetic field.

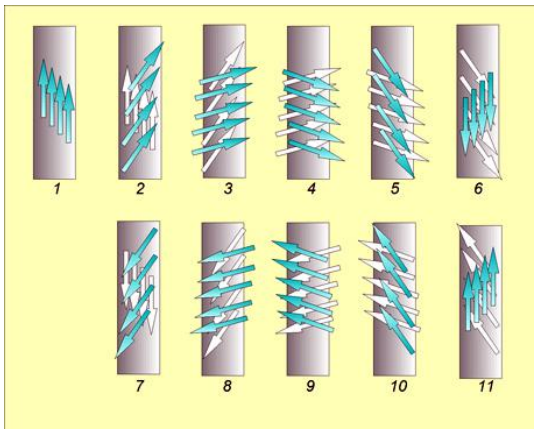

Fig. 5: The pitch angle of the helical total magnetic field, $\boldsymbol{B}$ vector, that encircles a field-aligned current changes continuously with increasing radial distance from the central axis of the current. There are no abrupt quantum jumps or breaks in this angle's change or in the field's magnitude. One cycle (0°–360°) of the pitch angle is shown. The cycle is sketched at eleven incrementally increasing sample values of radius. The shaded arrows show the total magnetic field direction at each value of radius, r, and the white arrows show the field direction at an increment just below each of those values of radius.

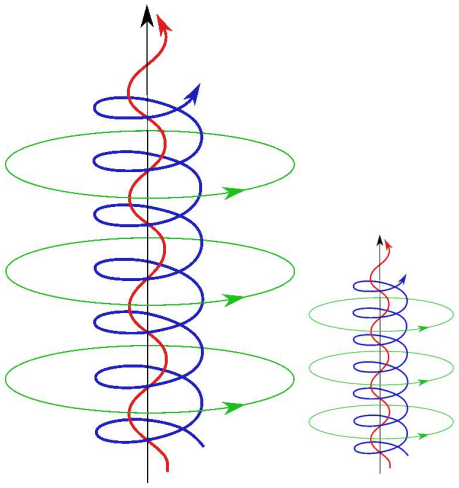

Fig. 6: Two different sized scale models of a FAC. These are both Lundquist-Alfvén-type images showing the helical structure of the collinear $\boldsymbol{j}$ and $\boldsymbol{B}$ vectors for small values of radius, r. (Left: Using $\alpha = \alpha_o$. Right: Using $\alpha = 2\alpha_o$.) This demonstrates why some investigators say that alpha controls the "tightness of twist". It only appears to do that as a secondary effect because it's primary effect is as a scale factor on the overall dimensional ***size*** (r, z) of the model's structure.

The entirety of this paper up to this point has been focused on the consequences of the reduction or possible elimination of the Lorentz $\boldsymbol{v}\times\boldsymbol{B}$ forces as defined in the second term of (3). But, the first term in that expression produces an independent, conduction component of the current density that may be added, via superposition, to the current density, $\boldsymbol{j}_z$, that has been derived above. This additional term is written as,

$$j_{cond} = q\boldsymbol{E}\left(\sum_k n_k \mu_{ions}^{(k)} + n_e \mu_e\right) \qquad (53)$$

where n_k is the ion density, with k = ionization number of the various ions, n_e is the electron density and $\mu_{ions}^{(k)}$ and μ_e are the respective mobilities of those ions and electrons in the plasma. Expression (53) is the point form of Ohm's Law. Another way that $\boldsymbol{j}_z$ might become increased is by narrowing the cross-sectional area of a Birkeland current as it squeezes down into a polar cusp in a geomagnetic field.

It is not known if any actual, observed cosmic currents are in the complete minimum (Lorentz force) energy, field-aligned state. Several apparently show evidence of near-force-free behavior [31]. In the steady-state minimum energy FAC configuration, all Lorentz forces have been eliminated and charge simply follows the magnetic field structure. For example, in Figure 3, any positively charged matter located at $r = 158$, has counter-clockwise motion.

The image shown in Figure 8 was obtained in a plasma laboratory. Neither this nor the image of Saturn's north pole in Figure 7 represent force-free currents because they both are images of collisions of such currents with material objects.

Figure 8 suggests what may occur if such an overall current density increase were to occur. The force-free structure would begin to undergo changes (if not be totally destroyed). Exactly what would happen is pure conjecture but if we start with Figure 3 and consider what might occur if and when a low intensity stream of positive charge begins to infuse the entire cross-section in a $+z$ direction (away from the reader), these additional positive charges would likely be deflected by Lorentz forces as follows (see Figure 3). At radii 33, 116, and 199 – deflection inward and clockwise. At radii 74, and 158 – deflection outward and counter-clockwise.

The two paths (inward and clockwise at $r = 116$ and the one at $r = 74$ moving outward and counter-clockwise) might appear to be a single path spiraling inward from $r = 116$ toward $r = 74$. Such pathways are suggested in Figure 8. Clearly in that state, the system is no longer at minimum energy – Lorentz forces are at work within the no-longer force-free plasma.

Another effect of an increase in the magnitude of the axial component of the current density, j_z, would be to add a small incremental vector in the $+z$-axis direction to each existing $\boldsymbol{j}_z$-vector. For example, consider sub-figures 2-5 in Figure 5. A small $+\boldsymbol{j}_z$ vector added to each of the shaded $\boldsymbol{j}$-vectors shown there would tend to twist them slightly counter-clockwise, away from being aligned with their corresponding $\boldsymbol{B}$-vector that remains fixed. The resulting Lorentz force ($\boldsymbol{j}\times\boldsymbol{B}$) would be directed inward (away from the viewer). However, if a similar small $+\boldsymbol{j}_z$ vector were to be added to each of the shaded $\boldsymbol{j}$-vectors shown in sub-figures 7-10 in Figure 5, this would

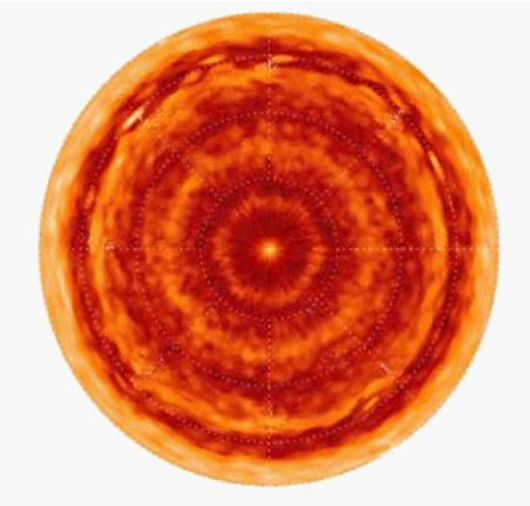

Fig. 7: Saturn's north pole, infrared Cassini image. Saturn is a gaseous planet composed mainly of hydrogen and helium. This image was obtained during the dark winter. The pole is encircled by a hexagonal feature in its atmosphere, which is thought to be caused by a planetary (atmospheric) wave. Image obtained using the infrared mapping spectrometer on board the Cassini Orbiter spacecraft. Courtesy of: NASA/JPL-Caltech/University of Arizona. The Cassini-Huygens mission is a cooperative project of NASA, the European Space Agency and the Italian Space Agency. Image Credit: NASA/JPL/GSFC/Oxford University/Science Photo Library [40].

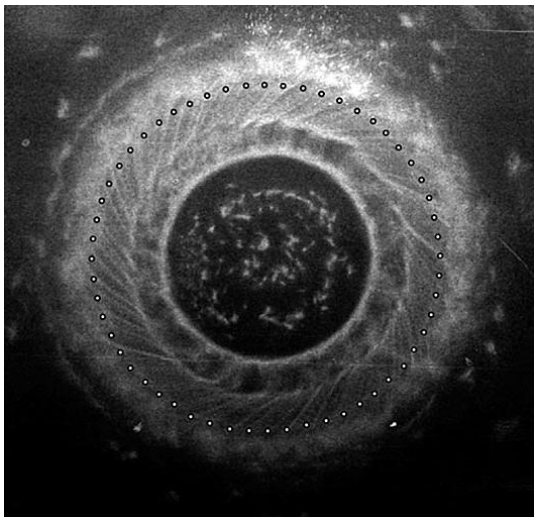

Fig. 8: Cross-section of a dense plasma focus Birkeland Current carrying $I = 174,000$ amperes. This image was captured by a witness plate placed in the discharge in a plasma lab. The spiral structure of the cross-section is visible. The 56-dot circular overlay shows the locations of the apparent spiral shaped paths of matter. Courtesy of A.L. Peratt, from Characteristics of a High-Current, Z-Pinch Aurora As Recorded in Antiquity, Part II Directionality and Source by Peratt, Directionality and Source. IEEE Transactions on Plasma Sci., August 2007 [41].

twist them slightly clockwise and the Lorentz force would, at those points, be directed outward (toward the viewer). Ions, then, will be pushed inward over radial ranges wherever azimuthal magnetic field, $\boldsymbol{B}_\theta$, is directed clockwise in Figure 3. Ions will be expelled outward wherever $\boldsymbol{B}_\theta$ is directed counter-clockwise in Figure 3. Matter (ions and neutral dust) will thus tend to congregate at intermediate radius values such as $r = 0, 94$, and 178. These are radii defined by the *odd zeros of* $J_1 = J_1(x) = J_1(\alpha r)$, $(x = 0, 7, 13, \dots)$ (see Figure 4 and column 3 of Table I for values). Electrons moving in the $-z$-direction will tend to be scavenged into the same r-regions. These are hollow cylindrical surfaces where $+\boldsymbol{j}_z$ dominates.

10 Comparison of results with observations

Images in Figures 7, 9, and 10 are obtained from actual astronomical observations. The image shown in Figure 7 is consistent with the hypothesis that Saturn is receiving a flow of electric charge via a Birkeland current directed into its north pole much as Earth is known to be experiencing. It is well known that currents in plasma drag un-ionized (as well as ionized) matter along in their path [42]. Figure 3 and the discussion at the end of Section 9, above, imply that clockwise and counter-clockwise counter-rotating current paths such as those at $r =$ 33 and 74 ought to exhibit such counter-rotation. But, for years it has been unknown whether the spiraling/circular paths appearing in Figures 7, 8 and 9 are really counter-rotating. It would require a video to reveal that relative motion.

It so happens that NASA has produced exactly such a video clearly showing counter-rotating (plasma) clouds within what appears to be the hexagonal shape at Saturn's north pole (see: [43] NASA video - Saturn's Hurricane). In this video, the term hurricane is used repeatedly by the narrator who expresses concern about the fact that the "storm" is fixed to the planet's north pole and that no water ocean exists below it to cause it to exist. He does not mention that actual hurricane winds do not counter-rotate as these do.

In that video, in shear regions between counter-rotating shells, what appear to be diocotron instabilities are visible (see Figure 9). Without NASA's video, the counter-rotational motions of these areas in the Saturnian surface would not be observed and therefore their existence would go undiscovered. This recent motion picture is crucial evidence of part of what is being presented here. Many other edited versions of the original NASA video exist that do not show counter-rotation taking place. The uncut original does.

11 Conclusions

It has been well-known for decades that the Lundquist solution (15) constitutes a simple model of a cylindrical force-free, field-aligned current. This model:

1. Dictates that the two vector fields $\boldsymbol{j}(r, \theta, z)$ and $\boldsymbol{B}(r, \theta, z)$ be everywhere collinear;

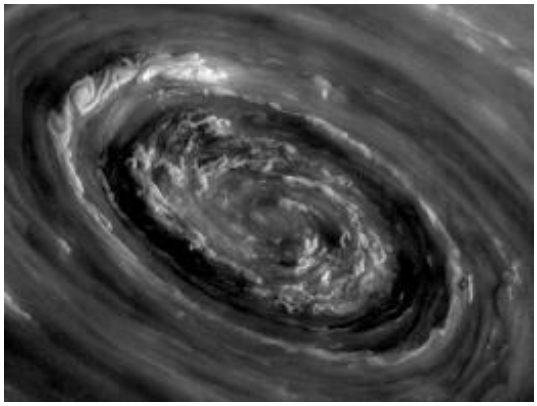

Fig. 9: Series of diocotron (shear) instabilities, especially obvious in the upper left of this image. This was taken from the NASA video [43] which clearly shows counter-rotation. From NASA Cassini mission video of Saturn's North Pole. Courtesy of: NASA/JPL-Caltech/University of Arizona. The Cassini-Huygens mission is a cooperative project of NASA, the European Space Agency and the Italian Space Agency. The imaging operations center is based at the Space Science Institute in Boulder, Colo. The Visual and Infrared Mapping Spectrometer team is based at the University of Arizona [43].

2. States that the overall solutions that specify the spatial dependence of those fields' magnitudes and directions are Bessel functions;
3. Assumes α is constant inside the plasma.

In this present paper we present a simple, but detailed derivation of this model of a force-free current and demonstrate, through straightforward mathematical analysis and strict adherence to the principles delineated in Maxwell's equations [35], a number of significant characterizations [44] of these field equations that are in strong agreement with reliable imagery obtained from both actual observations of phenomena in space and measurements in experiments in plasma laboratories. The most significant of those results are:

1. The complete mathematical model of a cylindrical, force-free FAC, including expressions for its current-density field is presented by (47)–(50), not just (15).
2. Magnetic fields produced by force-free currents stretch out radially from the central axis of the current stream much farther, and with greater effect, than previously thought. For radial distances, r, within the plasma ($r < R$) the amplitudes of those helical fields decay slowly *in inverse proportion to the square root of* r.
3. The fact that expression (23) requires that no component of the magnetic field, $\boldsymbol{B}$, can extend outward in the radial direction (and the fact that $\boldsymbol{B}$ and $\boldsymbol{j}$ are everywhere collinear) demonstrates that no dissipative currents or fields leave the cylindrical structure along its length. Birkeland's critics thought that the final, relaxed distribution would be an infinite dispersion, not a strong, tight cylinder (which it is).
4. The structural stability of the spiraling fasces-like wrapping of the magnetic field explains the observed enigmatic stability of Birkeland currents over long inter-planetary, inter-stellar, and inter-galactic distances. For example, the cosmic current "jet" emanating from galaxy M87 remains collimated over a distance exceeding 5000 light years [46]. The stability of the flux-rope connecting the Sun and Earth is now better understood (see Section 8).
5. The angle of pitch of the helix varies smoothly and continuously with increasing radial distance, r, from the central axis of the current out as far as the plasma's current-carrying charge density extends. This causes cyclical reversals of direction (counter-flows) in both the axial and azimuthal magnetic field and its collinear current density. The magnitude of both the $\boldsymbol{B}$ and $\boldsymbol{j}$-fields may be greater than zero for r values far beyond the first zero of $J_0(\alpha r)$ (which occurs at $r = 2.4048/\alpha$). Figure 6 is shown to be correct but incomplete, and thus potentially misleading.
6. Coupled with the new NASA video of Saturn's north polar region, this presentation strongly supports the hypothesis that a Birkeland current is feeding electric current into that region.
7. Parameter α controls the size of the resulting model in both the r and z dimensions (together – not separately). The value of α is arbitrary and is selected to enable the model to fit the size of the actual space-plasma being modeled.
8. The major difference between a field-aligned current (FAC) and a Birkeland current is that in a FAC the total current, $\boldsymbol{I}$, is a minimum. When the current density at any point, $\boldsymbol{j}$, increases for any reason above its minimal value, non-zero Lorentz forces begin to occur and the matter scavenging described in Section 9 takes place.
9. The mathematical procedure offered here is circumscribed to an extent not typical of other papers by caveats regarding the consequences of the universal unquestioning acceptance of the generality of the expression $\mu\boldsymbol{j} = \alpha\boldsymbol{B}$ (14). This is not applicable in filamented plasma.

The conclusions drawn from the analysis of the mathematical model derived in this paper have been tested against original motivating observations and measurements. Consistently strong agreement is found. Many otherwise enigmatic images stand witness to the potential benefits of considering possible electrical causation of other cosmic plasma phenomena.

The M2-9 Hourglass planetary nebula in Figure 10 is a prime case in point. We suggest that the narrowing of the

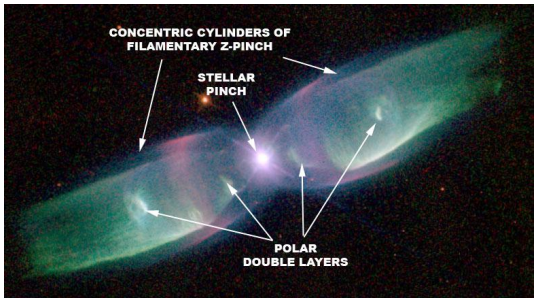

Fig. 10: The Hourglass (or Butterfly) planetary nebula, M2-9. In this image the separate hollow, cylindrical tubes of matter are clearly visible. The cross-sectional area of the structure diminishes near the center of the pinch. Since the total current is the same at every cross-section, this means regions near the central pinch have increased current density (A/m^2) and corresponding greater visual brightness. Courtesy of the Hubble Legacy Archive, NASA, ESA Processing *Judy Schmidt*. The Hubble Legacy Archive (HLA) is designed to optimize science from the Hubble Space Telescope by providing online, enhanced Hubble products and advanced browsing capabilities. The HLA is a joint project of the Space Telescope Science Institute (STScI), the Space Telescope European Coordinating Facility (ST-ECF), and the Canadian Astronomy Data Centre (CADC) [45].

plasma FAC channel due to the z-pinch creates an increased current density which causes a transition of the plasma from the dark mode into the visible glow and arc modes. The observed dual, concentric cylinders of excited plasma are consistent with the counter-rotation, matter scavenging, and reversing flows described in this paper.

Acknowledgements

The author wishes to express his sincere thanks to Dr. Jeremy Dunning-Davies for recognizing that the differential equation derived in this study is a Bessel Equation, whose solutions are given by the Bessel functions, J_0 and J_1. He also gave the author much appreciated encouragement and very much needed advice.

Dr. Timothy Eastman, Wyle senior scientist at NASA Goddard, Dr. Ron DeLyser, EE Department U. of Denver, Dr. C. J. Ransom of Vemasat Labs, Dr. W. A. Gardner, and Dr. Michael Clarage gave freely and graciously of their time, advice, and assistance to help in this effort.

Submitted on: January 27, 2015 / Accepted on: February 17, 2015
First published online on: February 20, 2015

References

1. Birkeland K. The Norwegian Polaris Expedition 1902–1903, Vol. 1, Sect. 1. Aschehoug, Oslo, Norway, 1908.
2. Lerner E. The Big Bang Never Happened. New York, 1991. p. 181.
3. Lundquist S. Magneto-hydrostatic fields. *Arch. Fys.*, 1950, v. 2, 361.
4. Lundquist S. On the stability of magneto-hydrostatic fields. *Phys. Rev.*, 1951, v. 83 (2), 307–311. Available online: http://link.aps.org/doi/10.1103/PhysRev.83.307.
5. Chandrasekhar S. and Kendall P. On force-free magnetic fields. *Astrophys. J.*, 1957, v. 12 (6), 457.
6. Gold T. AAS-NASA Symposium on Physics of Solar Flares. Hess W. N., ed., NASA SP–50, 1964, p. 389.
7. Alekseev I. and Shabansky V. A model of a magnetic field in the geomagnetosphere. *Planet. Space Sci.*, 1972, v. 20, 117.
8. Chiu Y. and Hilton H. Exact Green's function method of solar force-free magnetic-field computations with constant alpha. I. Theory and basic test cases. *Astrophys. J.*, 1977, v. 212, 873–885.
9. Cloutier P. and Anderson H. Observations of Birkeland currents. *Space Sci. Rev.*, 1975, v. 17, 563–587.
10. Alfvén H. Evolution of the solar system. Scientific and Technical Information Office National Aeronautics and Space Administration, Washington, D.C., 1976.
11. Hasegawa A. and Sato T. Generation of Field Aligned Current during Substorm in Dynamics of the Magnetosphere. Akasofu, S-I., ed., D. Reidel, Hingham, MA, 1979, p. 529.
12. Nakagawa J. and Raadu M. A. On practical representation of magnetic field. *Solar Phys.*, 1972, v. 25, 127.
13. Olson W. A model of distributed magnetospheric currents. *J. Geophys. Res.*, 1974, v. 79, 3731.
14. Rostoker G., Armstrong J. C., and Zmuda A. J. Field-aligned current flow associated with intrusion of the substorm-intensified westward electrojet into the evening sector. *J. Geophys. Res.*, 1975, v. 80, 3571–3579.
15. Zmuda A., Armstrong J. C., and Heuring F. Characteristics of transverse magnetic disturbances observed at 1100 kilometers in the auroral oval. *J. Geophys. Res.*, 1970, v. 75 (25), 4757–4762.
16. Dessler A. Corotating Birkeland currents in Jupiter's magnetosphere - An Io plasma-torus source. *Plan. Space Sci.*, 1980, v. 28, 781–788.
17. Harel M., Wolf R. A., Reiff P. H., Spiro R. W., Burke W. J., Rich F. J., and Smiddy M. Quantitative simulation of a magnetospheric substorm 1. Model logic and overview. *J. Geophys. Res.*, 1981, v. 86, 2217–2241.
18. Alissandrakis C. On the computation of constant alpha force-free magnetic field. *J. Astron. Astrophys.*, 1981, v. 100 (1), 197–200.
19. Burlaga L. Magnetic clouds and force-free fields with constant alpha. *J. Geophys. Res.: Space Phys.*, 1988, v. 93 (A7), 7217–7224.
20. Durrant C. J. Linear force-free magnetic fields and coronal models. *Aust. J. Phys.*, 1989, v. 42, 317–329.
21. Falthammer C. G. Magnetosphere-Ionosphere interaction. Near-Earth Manifestations of the plasma universe. *IEEE Trans. Plasma. Sci.*, 1986, v. 14 (6), 616–628,
22. Potemra T. Birkeland Currents I. The Earth's Magnetosphere (From a special issue dedicated to Hannes Alfvén on his 80th Birthday). *Astrophys. Space Sci.*, 1988, v. 144 (1–2), 155–169.
23. Potemra T. Observation of Birkeland currents with the TRIAD Satellite. *Astrophys. Space Sci.*, 1978, v. 58 (1), 207–226.
24. Potemra T. Alfvén Waves and Birkeland Currents. *Physica Scripta*, 1995, v. T60, 107–112.
25. Botha G. J. J. and Evangelidis E. A. Cylindrical linear force-free magnetic fields with toroidal flux surfaces. *Mon. Not. Roy. Astron. Soc.*, 2004, v. 350 (1), 375–384.
26. Romashets E. and Vandas M. Force-free magnetic field in a cylindrical flux rope without a constant alpha. *Adv. Space Res.*, 2005, v. 36 (12), 2268–2272.
27. Eastwood J. Flux ropes. NASA Goddard, 2009.
28. Goedbloed J. and Poedts S. Principles of Magnetohydrodynamics: With Applications to Laboratory and Astrophysical Plasmas. Cambridge University Press, Cambridge, UK, 2004.
29. Biskamp D. Nonlinear Magnetohydrodynamics. Cambridge University Press, Cambridge, UK, 1997.

30. Ferraro V. and Plumpton C. An Introduction of Magneto-Fluid Mechanisms. Clarendon Press, Oxford, 1966.

31. Peratt A. Physics of the Plasma Universe. Springer-Verlag, New York, 1992, p. 44. Republished ISBN 978-1-4614-7818-8, 2015, p. 406.

32. Titov V., Török T., Mikic Z., and Linker J. A. A method for embedding circular force-free ropes in potential magnetic fields. *Astrophys. J.*, 2014, v. 790 (2), 163.

33. Yang Y. Y., Shen C., Zhang Y. C., Rong Z. J., Li X., Dunlop M., Ma Y. H., Liu Z. X., Carr C. M., and Rème H. The force-free configuration of flux ropes in geomagnetotail: cluster observations. *J. Geophys. Res.: Space Phys.*, 2014, v. 119 (8), 6327–6341.

34. Eastman T. Wyle Senior Scientist at NASA Goddard, Personal communication, 5 February 2015.

35. Jackson J. Classical Electrodynamics, 2nd ed. John Wiley, New York, NY, 1975.

36. Callen H. Thermodynamics and an Introduction to Thermostatistics, 2nd ed. John Wiley, New York, NY, 1985.

37. Wiegelmann T. and Sakurai T. Solar force-free magnetic fields. *Living Rev. Solar Phys.*, 2012, v. 9 (5). Available online: http://solarphysics.livingreviews.org/Articles/lrsp-2012-5/.

38. Alfvén H. Cosmic Plasma. D. Reidel, Hingham, MA, 1981, p. 97.

39. Matlab, Bessel functions of the First and Second Kind. Available online: http://www.mhtlab.uwaterloo.ca/courses/me755/web_chap4.pdf.

40. Infrared image of Saturn's North pole. Available online: http://www.sciencephoto.com/media/326994/view, 4 February 2015.

41. Peratt A. Image: Penumbra from a dense plasma focus device. Available online: http://www.academia.edu/9156605/Neolithic_rock_art_associated_with_intense_auroral_currents, Figure 51, 4 February 2015.

42. Mehdipour H. and Foroutan G. The magnetized sheath of a dusty plasma with nanosize dust grains. *Phys. Plasmas*, 2010, v. 17, 083704.

43. NASA video of the Saturn hurricane. Available online: http://www.jpl.nasa.gov/video/details.php?id=1213, 4 February 2015.

44. Scott D. Real properties of electromagnetic fields and plasma in the cosmos. *IEEE Trans. Plasma Sci.*, 2007, v. 35 (4), 822–827.

45. High resolution NASA image of the Hour-Glass or Butterfly planetary nebula M2-9. Available online: http://apod.nasa.gov/apod/ap130915.html, 4 February 2015).

46. Messier 87 - SEDS catalog. Available online: http://messier.seds.org/m/m087.html.